Characterization of friction force dynamics

Farid Al-Bender, Jan Swevers

Characterization of Friction Force Dynamics

Behavior and modeling on micro and macro scales

Farid Al-Bender, Jan Swevers

farid.al-bender@mech.kuleuven.be

tel:+32/16/322480

Friction modeling has been steadily gaining in interest over the last two decades. Despite persistent and painstaking efforts, however, no satisfactory, comprehensive, practicable friction model that captures all of the experimentally observed aspects of friction force dynamics in one formulation is available. Friction comprises multiscale processes requiring multiscale theories [1]. Such theories are not fully developed, however, and the significance of each theory at each level is not fully understood. Thus, most available friction models are, in essence, empirical, that is, based on limited observations and interpretations. In this sense, the resulting models are valid only for the specific scope of test conditions, such as the level and type of excitation, used to obtain the data. On the other hand, the development of simulation models and, where possible, predictive theories, at scales from atomic, through continuum, to useful engineering models, can fill gaps in the toolboxes available to designers and analysts.

This article presents an example of comprehensive model-building, which starting

from the generic mechanisms behind friction, leads to the construction of a model that explains observed macroscopic friction behavior. Effective physics-based models at multiple scales can facilitate future work on the inter-relationships among models by furthering the understanding of emergent, collective frictional properties. Moreover, predictive physical models facilitate the derivation of simple models for control purposes. An example is the generalized Maxwell-slip model, which is discussed in this article.

Considering friction as a mechanical system, a close examination of the sliding process reveals two friction regimes, namely, the pre-sliding regime and the gross sliding regime. In the pre-sliding regime the adhesive forces owing to asperity contacts are dominant, and thus the friction force is primarily a function of displacement rather than velocity. The reason for this behavior is that the asperity junctions deform elasto-plastically, thus behaving as nonlinear hysteretic springs. As the displacement increases, more and more junctions break and have less time to reform, resulting eventually in gross sliding. The sliding regime is, thus, characterized by a continuous process of asperity junction formation and breaking such that the friction force becomes predominantly a function of the relative sliding velocity [2]. The transition from pre-sliding to gross sliding is a criticality that depends on many factors such as the relative velocity and acceleration of the sliding objects [3],[4].

Besides the field of tribology, where the origin of friction is one of the main topics, modeling and compensation of friction dynamics are treated in several other domains. In the machining and assembly industry, the demand for high-accuracy positioning systems and tracking systems is increasing. Research on controlled mechanical systems with friction is motivated by the increasing demand for these systems. Friction can severely deteriorate control system performance in the form of higher tracking errors, larger settling times,

hunting, and stick-slip phenomena [5],[6]. In the domain of structural dynamics the damping of large space structures is of interest. This damping is caused mainly by energy dissipation due to the pre-sliding displacement in mechanical joints, also known as structural damping. Geomechanics is concerned with the origin of earthquakes, which are stick-slip phenomena owing to the interaction of friction between tectonic plates. In short, friction is one of the main players in a wide variety of mechanical systems.

We divide approaches to friction modeling into two classes, namely, analytical and empirical. The physics-motivated approach starts at the micro-level of asperity interaction, with assumed physical phenomena governing the interaction forces, and synthesizes a mechanical system of friction. The resulting model can then be verified by the macroscopically observed friction force dynamics. Thus, while the basic mechanisms responsible for friction are phenomenological, that is, empirical, the resulting macroscopic behavior can be seen as an emergent behavior that varies qualitatively with the chosen the parameters of the micro-process. The purpose of this modeling approach, which is popular in tribology [7], atomic friction [8], and geomechanics [9], is to gain insight into the mechanisms determining friction behavior. For details on the various classes of this modeling approach, see “Physics-motivated Friction Models”. Finally, the generic, physics-motivated model outlined in the next section belongs to this category.

In contrast, empirical models look at the process from without and ask the following question: Which dynamical model can best account for observed macroscopic frictional behavior, regardless of what the actual physics of the problem might be? The purpose of these models is then to capture as many friction properties as possible in one formulation with a minimum set of parameters, which remain to be determined. Owing to their simplicity,

the resulting models are appropriate for quick simulation or control purposes. When their complexity increases, empirical models can approach, in terms of predictive power, physics-based models, as shown in [10]. Despite that fact, empirical models do not predict the behavior from the internal physics of the problem, but rather from dynamical systems consideration. Analysis of various empirical friction models reveals an underlying general model structure. For details, see “Generalized Empirical Friction Model Structure”. For an overview of the development of empirical models, see “Empirically Motivated Friction Models”.

The underlying aim of this article is to develop a link between the physics-based and empirical approaches. In particular, we first present a generic, physics-based friction model, and then deduce a simple empirical formulation based on the results obtained from the physics-based model. Finally, the simulation results obtained from both models are compared with experimental observations.

A GENERIC FRICTION MODEL BASED ON PHYSICAL PHENOMENA

In order to formulate a generic friction model (GFM), we begin by considering two multiscale rough surfaces, belonging to two solid, elastic bodies, in contact with each other without sliding and under a static compressive force F_n. Since the surfaces are not smooth, contact occurs only at discrete points that sustain the total compressive force. The spatial randomness of the contact points corresponds to the nature of surface roughness, whereas the different sizes of the contact spots are due to the multiple scales of roughness. For a given load, the spot size depends on surface roughness and the mechanical properties of the contacting bodies. It is evident that even for a regular surface, the shapes of the contact spots are not homogeneous and can be irregular and complex.

When two surfaces slide relative to each other, a tangential friction force F_f is experienced. This force is the result of *adhesion* and *deformation* arising from asperity interactions. Adhesion refers to the tangential (that is, shear) surface forces arising from various of sources when the surfaces are within a certain proximity of each other. Thus, short range, metallic and covalent bonding forces are considered as well as long range adhesion forces, such as van der Waals [11], [12]. Deformation losses, in metals, are of a rate-independent hysteretic nature [13], in the near-surface material, as a consequence of geometrical deformation of asperities. Deformation losses take place during interlocking of asperities, and persist until after the asperities pass over each other. This phenomenon is akin to structural damping. A third fundamental mechanism, which is more directly responsible for friction dynamics, is *creep* of the contact in the normal direction. This phenomenon is best imagined as follows. Two rough surfaces that are loaded against each other tend to sink into one another over time, leading to increased asperity interlocking and, thus, to higher tangential forces upon sliding. These mechanisms comprise the first category of ingredients of the physics-based model.

The adhesion, deformation, and creep mechanisms may be interconnected with each other to the degree that it is difficult to draw a clear boundary between the spheres of influence of each. We assume a priori the existence of these mechanisms, consider them abstractly, and lump adhesion and creep, expediently, into one parameter. This parameter is a time-increasing local adhesion coefficient. Deformation losses, on the other hand, are quantified by the loss of stored elastic of the deforming asperities. Thus, by varying the parameter responsible for each mechanism, we can gain insight into its effect on the global friction behavior.

The dynamic interaction of these three mechanisms with the asperity mass and stiff-

ness is responsible for the richly varied and complex behavior of the friction force. This interaction is brought about mainly by the continually changing contact topography, in time and relative displacement. This category of ingredients, called the *asperity interaction scenario*, is equally significant in determining the friction force dynamics. This scenario considers the normal and tangential deformation of asperities of both surfaces as a function of the relative tangential translation between the two objects, while the normal distance between remote points in the two objects remains constant. Modeling the contact between two rough elastic surfaces is often reduced to modeling the contact of one elastic surface, having the equivalent roughness and elasticity of both surfaces, with a rigid perfectly flat second surface [13], [14], [15]. While such a reduction is acceptable when considering quasi-stationary contact during pre-sliding, this approach falls short of revealing the dynamics of the nonstationary case, that is, sliding, since it masks the interlocking of asperities and gives a false picture of the continually changing relative topography and hence of the resulting tangential forces. In practice, quantification of the two sets of ingredients for a given contact may not be obvious. However, since we are concerned with the qualitative, model-structure aspects of friction force dynamics, this issue is outside the scope of this article.

Having identified the ingredients, the next step is to formulate a spatially distributed model by applying these ingredients to a large population of individual idealized asperities that vary randomly. In particular, the contact surfaces of two blocks rubbing against each other can be represented, after transformation, as follows. One flexible surface, being chosen for convenience to be the upper surface, containing all equivalent asperities, each with its own stiffness, mass, and shape, interacts with a rigid, rough (that is non-flat) lower surface. Thus, although both surfaces contain asperities, all of the asperity dynamics are assigned to the upper surface.

Figure 1(a) depicts the life cycle of an upper-surface asperity, where it is assumed that the upper surface is moving from left to right with respect to the fixed lower surface. Although topographical characteristics are assigned to both surfaces, the equivalent interaction characteristics, namely, stiffness, mass, compression, and adhesion, are lumped into one point on the upper surface. This point is initially moving freely, until it touches the lower rigid surface. After sticking and slipping over the lower profile, the asperity breaks completely loose from the lower profile. In doing so, the asperity is assumed to dissipate all of its elastic energy through internal hysteresis losses. Figure 1(b) depicts the tangential, hysteretic deformations that the asperity undergoes. In case the asperity touches the lower surface, it is said to be in an *active* state. For the other cases, the asperity is *inactive*. This scenario is reminiscent of the Tomlinson-Prandtl atomic model [16], except that our scenario accounts for creep, adhesion, and loadcarrying, which are essential in revealing friction force dynamics. In this formulation, the possible vibration of an asperity during contact is ignored.

From the moment the asperity becomes active, it begins to follow the profile of the lower surface, by deforming normally through ζ and tangentially through ξ, resulting in normal and tangential forces. The normal force is given by

$$F_n(t) = k_n \zeta(t),$$

while the tangential force is given by

$$F_t(t) = k_t \xi(t),$$

where k_n and k_t equal the normal and tangential stiffness of the equivalent asperity, respectively. The maximum tangential force $F_\mu(t)$ an asperity can sustain before slipping equals the adhesion force, that is,

$$F_\mu(t) = \mu(t) k_n \zeta(t),$$

where the local adhesion coefficient $\mu(t)$ is function of the contact time, owing to normal creep. This behavior can be deduced from the relation between static friction and dwell (rest) time. Coulomb in 1785 [17] is probably the first to explore this time dependence [18]. As a rule, the static friction force F_s increases with dwell. An overview of various formulae for this time dependence is given in [11].

Thus, depending on the relative values of ζ, μ, k_n, and k_t, the asperity tip initially *sticks* (case (iia) in Figure 1(b)) to the lower profile, *slips* on the profile, and, finally, breaks loose from the profile. Assuming, without loss of generality, linear tangential and normal elasticity of the upper asperity, the force initially increases linearly with the displacement until slip occurs. In the meantime, $\mu(t)$ keeps increasing with contact time. Once the asperity breaks loose from the lower surface, its tip vibrates tangentially and normally, thereby dissipating, partially or fully, its elastic energy, through internal hysteresis, until it comes to rest or comes in contact with the next surface profile. For low sliding speeds and large separation of consecutive asperities, as compared to asperity size, all of the tangential elastic energy is assumed to be lost. Besides the deformation and adhesion of the equivalent asperity, the mass can contribute also to the friction force. When the equivalent asperity comes into contact with the surface profile, the asperity undergoes an impulse, resulting in an energy equal to $mv^2/2$, with v the relative velocity of the equivalent asperity.

To investigate the various types of friction behavior that the GFM can simulate at the macroscopic level, between 1000 and 4000 equivalent asperities are simulated. A rubbing contact is modeled as that taking place between one flat object covered by a population of mutually independent elastic point asperities with randomly chosen constant heights h, masses m , normal stiffnesses k_n, and tangential stiffnesses k_t. On the other side, a rigid surface

having, for each asperity, a square wave profile (dashed line of Figure 1(a)) with constant height but randomly chosen wavelengths w, which are fixed during the lifetime of a single asperity contact. The stochastic distribution functions of the parameters h, m, k_n, k_t, and w, which depend on the actual contact considered, influence the resulting friction dynamics. The mean ratio between the characteristic length of inactivity and activity is given by a topography factor α. The shape of the local adhesion coefficient is chosen to be an exponential saturation function, which is identical for all of the asperities.

As shown in Figure 1, the asperity can tilt so that its load-carrying capacity can also vary as a function of the position of its tip relative to its base. This situation leads to normal-force dynamics, called the *lift-up* effect [7], which is not considered further in this article owing to its lesser relevance.

TYPES OF FRICTION BEHAVIOR

We now consider the behavior of the GFM for several well-established characteristics of dry friction. These characteristics are the pre-sliding hysteresis characteristic, velocity weakening and strengthening, the dynamical behavior of the friction force in the velocity during gross sliding, and the transition between pre-sliding and gross sliding. The implementation of the model is discussed in [7].

To specify the contact considered, the user must provide values for the normal and tangential stiffness of the population of asperities, their mass distribution, the surface topography parameters, and the local adhesion coefficient function. As input to the sliding case to be examined, the normal proximity between the surfaces and the tangential motion

trajectory must be given. The output of the model is then the friction and normal forces, whose dynamics are discussed in the following sections.

The parameters of the GFM used to simulate the macroscopic behavior are purposefully chosen to be rather unrealistic in order to exaggerate their effects for better visualization. All of the results are expressed in normalized, dimensionless units. This normalization is performed with respect to a set of reference parameters of the interacting surfaces [7]. We thus focus on the qualitative behavior of the friction. The real scale of the figures, that is, the quantitative behavior, depends on the material combination and surface topography, which can be varied for the purpose of simulation.

Pre-sliding behavior

At very small displacements, that is, in the pre-sliding regime, experiments reveal a hysteretic displacement-dependent friction force [19], [20], [21], [3]. Figure 2 shows the results obtained by the GFM. The position signal is chosen to generate an inner loop within the outer hysteresis loop. The resulting friction-position curve is rate independent. In other words, the friction-displacement curve is independent of the speed of the applied displacement signal. This is one property of hysteresis. When the inner loop is closed, the curve of the outer loop is followed again until that is also closed. This, property of hysteresis is known as the *nonlocal memory* characteristic. Besides being experimentally demonstrated, see, for example, [3], this property can be shown, by theoretical analysis, to hold for any contact or phenomenon that is based on the Maxwell-slip model [22]. Conversely, the Maxwell-slip model represents an approximation to the physics of an elastic asperity that slides on a plane subject to the Coulomb friction law, see section ”A reduced friction model for simulation and

control". Since the GFM approximates the Maxwell-slip model for sufficiently small relative displacements, it is natural to expect that the GFM also satisfies the nonlocal memory property for small displacements.

The shape of the hysteresis function is determined by the distribution of the asperity heights, the tangential stiffness, and the normal stiffness. This hysteresis behavior arises, in the present simulation, primarily from micro-slip, that is, the breaking of adhesive contacts, just as in the Maxwell-slip model discussed below. The contribution of deformation losses, which are hysteresis losses in the bulk materials, depends on the relative value of this part as compared to the adhesive part, as well as on the tangential stiffness of the asperities, which governs the extent of deformation before slip.

Gross sliding

The asperity contacts are continually being created and broken in the gross sliding regime. Two main characteristics are of interest here. The first is the steady-state friction force behavior with increasing steady-state sliding velocities, generally known as the Stribeck curve. The second is the dynamic change of the friction force due acceleration and deceleration, known as the *friction lag* or *friction memory* phenomenon.

Velocity weakening and strengthening in the Stribeck curve

When the friction force is measured at constant velocity values, the resulting functional relationship has a characteristic form. For increasing velocities, the friction force initially decreases to a minimum (*velocity weakening*) and then increases again (*velocity*

strengthening). In lubricated sliding, this characteristic is known as the Stribeck curve,where the velocity weakening arises from the initial buildup of hydrodynamic pressure, while the velocity strengthening is attributed to the viscous shear of the lubricating film. The same kind of behavior holds true for dry friction, although the mechanism causing it is different from the case of lubricated friction, which justifies using the same name, that is, the Stribeck curve, to describe it. In dry friction, velocity weakening is a consequence of the fact that adhesion has less time to build up when sliding velocity increases, while velocity strengthening arises from asperity inertia effects, which increase with increasing sliding velocity, see further below. Thus, the actual form of the friction-velocity curve is determined by various process parameters, namely, the normal creep or, equivalently, the time evolution of adhesion, the surface topography, and the asperity parameters, primarily the tangential stiffness and inertia [7].

Figure 3 shows the steady-state friction curve (curve 1), the Stribeck curve and its splitting-up into different components, namely, a component due to deformation of the asperities (curve 2), a component due to the adhesion forces (curve 3), and a component due to the impact of the asperity masses (curve 4). The first two components are decreasing functions of the velocity, whereas the last component is an increasing function of the velocity.

It may be obvious that, based only on measured curves such as curve 1 of Figure 3, it is impossible to distinguish the various components from one another. The effect of each component depends on the surface topography and the dynamic asperity properties, that is mass and stiffness.

Let us first examine the velocity weakening behavior. As shown above, this behavior

depends on the adhesion and deformation characteristics of the asperities. Figure 4 shows the velocity-weakening curves for various mean tangential stiffness values, with the asperity mass neglected. Decreasing friction force for increasing velocity is a consequence of the rising local adhesion coefficient as a function of the contact time. However, the magnitude of the friction force depends also on the elastic energy dissipated by an asperity, which decreases with increasing tangential asperity stiffness. This velocity-weakening behavior is sometimes termed the *Stribeck effect*.

With regard to the origin of velocity weakening, a fundamental correlation exists between the coefficient of static friction, plotted as a function of the dwell time, and the coefficient of steady sliding, that is, kinetic friction, plotted as a function of the sliding speed [4], [23]. Taking the static-friction-versus-dwell-time behavior to be a measure of the local-adhesion-coefficient-versus-time characteristics, this correlation can be seen as the transformation

$$\mu_s \left(\frac{D_0}{t_{stick}} \right) = CF_f(v) \triangleq \mu_d(v),$$

where μ_s and μ_d are the static and the sliding friction coefficients, respectively, F_f is the kinetic friction force, t_{stick} is the dwell time, and C is a constant. The process characteristic number D_0 is the creep length, and D_0/v is the time needed to surpass an average asperity contact. Figure 5 depicts the above-mentioned correlation between the static and sliding friction coefficients, as simulated by the GFM, compared with experimental results. Note that two sets of data are plotted on each subfigure, namely, $\mu_d = CF_f$ as a function of v, and μ_s, which equals the local adhesion coefficient $\mu(t)$, as a function of D_0/t_{stick}.

Figure 5(a) shows simulated results using an exponential local-adhesion-coefficient curve, whereas Figure 5(b) shows the simulated curves using a logarithmic local adhesion

coefficient curve. Figure 5(c) shows experimentally measured curves from [4], correlating the static and the sliding friction coefficients. In all cases, the static and sliding values of the coefficient of friction lie approximately on the same curve. Figures 5(b) and 5(c) represent a special case, where the curve is a straight line for several orders of magnitude of the abscissa.

This discussion shows that velocity weakening will depend on the rate of change of the sliding velocity, see next section. This dynamics in the velocity does not hold for velocity strengthening to which we now turn.

In the above analysis, the mass of the equivalent asperity is assumed to be negligible. When the asperity inertia is taken into account, an kinetic energy component is added to the asperity dynamics. This energy yields a force that depends the sliding velocity. Consequently, this *velocity strengthening*, that is analogous to the *viscous effect* in lubricated friction, takes place instantaneously with the velocity change as noted above.

Friction lag

Friction lag, also called hysteresis in the velocity, or frictional memory, is manifested by a lag in the friction force relative to the sliding velocity. The origin of friction lag in lubricated friction [24], relates to the time required to modify the lubricant film thickness, which is known as the *squeeze effect*. Friction lag is also observed in dry friction experiments [4], where lubrication is not used. The mechanism causing friction lag in dry sliding is similar to that for lubricated friction, namely, that the local adhesion coefficient increases with the time of contact of two opposing asperities, owing to normal creep. In other words, time is required before the friction force changes with changing sliding velocity. Since the normal

creep is caused by the sinking of the surfaces into each other, this mechanism is akin to the squeeze effect in lubricated friction.

Figure 6 shows the friction force as a function of the velocity using the GFM. The applied velocity signal is sinusoidal, of various frequencies, plus a constant offset to ensure unidirectional motion at all times. Figure 6 shows that the friction force is higher for acceleration than for deceleration, so that the dynamic friction force curve circles around the steady-state curve. Figure 6 shows, moreover, that the departure from the steady-state curve becomes more pronounced and qualitatively different at higher acceleration levels.

A general empirical *rate-state*-dependent friction law is developed in [25] based on experiments involving a suddenly imposed step change in the velocity. The experiments in [25] suggest that the friction force response to the velocity step is a combination of an instantaneous increase with the velocity and a first-order-like decay with the evolving state. The first factor, namely, that the friction force increases simultaneously with the suddenly imposed increase of velocity, corresponds to the asperity inertia, that is, the viscous effect. The second factor results in a nonlinear lag response.

Using the GFM to simulate this behavior (see Figure 7(b)) the time lag can be approximated as a first-order system. However, the time constant depends not only on the velocity step, but also on the initial steady-state velocity. Figure 7(a) shows the response for the same velocity steps, when asperity inertia, that is, the viscous effect, is neglected. Clearly, the friction lag effect is independent of the asperity inertia, which can be seen to result in the instantaneous response of the friction force to velocity change. For this reason, the mass is neglected for the study of the friction lag in Figure 6, as well as for the study

of the transitional behavior from pre-sliding to gross sliding, as discussed below.

Transitional behavior

Most continuum models, such as the rate-state model, cannot deal with the behavior at transition from pre-sliding to sliding and vice versa. This transition behavior can be investigated by applying a periodic displacement signal to the system. Figure 8 shows the friction force as a function of a sinusoidal velocity excitation. Friction lag is evident in Figure 8, as well as the crossover at velocity reversals, passing through pre-sliding. When the velocity goes through zero (a), the direction of motion is reversed, and all of the active asperities are relaxed and reloaded in the new direction of displacement. The friction force increases until it reaches a maximum value (b), called the breakaway force, lying above the steady-state curve. From the moment of breakaway, the object is in gross sliding, and the friction force is attracted to the steady-state curve. As in the case of friction lag, the steady-state curve lies between the curves of acceleration ($b-c$) and deceleration ($c-d$). The results obtained by the GFM have the same qualitative behavior as the experimental results reported in [26], [3].

Stick-slip behavior

Figure 9 schematically shows a commonly used setup for inducing stick-slip motion. This setup comprises a block in contact with a fixed surface. The block is connected to a spring (and possibly a damper in parallel to it) whose free end is driven with a constant velocity v_0. The stick-slip oscillation is influenced not only by the nature of the surfaces in contact, but also by the dynamics of the mass-spring-damper system as well as the driving

velocity v_0. The negative slope in the friction-velocity curve is a necessary, but not sufficient, condition for oscillation around steady sliding .

Figure 10 shows the stick-slip response when the GFM model is used to simulate the friction interaction. The stick and slip phases are visible in Figure 10(a), where the friction force has the same time-dependent behavior as experimentally observed in [3]. In particular, the object sticks until the friction force equals the breakaway force. The block then begins to slide, and the increasing velocity results in a decreasing friction force. At the same time, the applied spring force decreases because the driving velocity v_0 is smaller than the velocity of the block. The block accelerates until the friction force equals the spring force. From that moment on, the block decelerates, resulting in a higher friction force, which maintains this process until the block sticks again. During the sticking period an oscillating behavior in the pre-sliding regime occurs. The frequency of this oscillation is determined by the mass of the moving object as well as the total stiffness of the spring and the contact stiffness in the pre-sliding regime. The damping of the oscillation is determined by the energy loss at the asperity contacts, which is given by the area enclosed by the hysteresis curve. Hysteretic energy loss is known as structural damping.

Figure 11(a) shows the time history of the states during stick-slip motion. The time variable, which is represented by the angle coordinate, is scaled by the mean period of one stick-slip cycle. Figure 11(b) is the corresponding phase portrait of the limit cycle.

Traction in rolling element systems

Most of the properties discussed above for gross sliding are equally applicable to the case of tractive rolling, that is, rolling with micro-slip. When an elastic body of revolution rolls over another, the traction field, that is, the tangential stress distribution, in the contact patch, changes progressively, with the distance traversed, from its initial, rest distribution until it reaches a steady-state distribution. This distribution, which is independent of the initial field prior to rolling, does not vary with further steady-state rolling. This eventual rolling regime is termed *gross* rolling; the time period building up to it, from commencement of rolling, is the *pre-rolling* regime. In the pre-rolling period, a region of micro-slip expands itself over a portion of the contact patch. Since the mechanisms governing the slip region are the same as those of sliding friction, the resultant traction in this regime is characterized by rate-independent hysteretic behavior with nonlocal memory as a function of the traversed displacement. This type of pre-rolling behavior [22], [27], [28] is shown [29], [30], [31] to have the characteristics of hysteresis with nonlocal memory. The gross-rolling dynamics show, however, only weak dependence on the velocity since the Stribeck curve is nearly flat for the low-level micro-slip velocities.

A REDUCED FRICTION MODEL FOR SIMULATION AND CONTROL

The GFM, though capable of simulating the nuances of friction-force dynamics, is too complex for simulation, identification, and control of systems with friction. In this sense, well-constructed empirical models have the advantage of capturing the basic characteristics of behavior in simple, tractable formulations. Thus, based on the results obtained from the GFM and on the formulation of empirical friction models given by (S1) and (S2)) of “Generalized

Empirical Friction Model Structure", we formulate a reduced friction model appropriate for quick simulation and control, named the generalized Maxwell-slip (GMS) model [32].

Since the Maxwell-slip model is a convenient way to model pre-sliding [22], [27], [28], [33], we use it as the starting point. The developed model is based explicitly on three friction properties, namely, a Stribeck curve for constant velocities, a hysteresis function with nonlocal memory in the pre-sliding regime, and friction lag in the sliding regime. Whereas the Leuven model tries to fit the hysteresis property into the rate-state sliding property, the GMS model works the other way around. In line with the physics of the problem, the GMS model imposes sliding dynamics onto the slip phase of the Maxwell-slip implementation of the hysteresis. As in the standard Maxwell-slip model shown in Fig. 12, the GMS model comprises a parallel connection of N single-state friction models, all having the same input and the same dynamics model, but with different parameter values. Each single-state friction model has a logic state that indicates whether the element is sticking or slipping. Letting v be the velocity input to the system and z_i ($1 \leq i \leq N$) the $i-th$ component of the state vector $\mathbf{z}$, the dynamics of each elementary model are determined by the following rules.

Rule 1: When the element sticks, the state equation is given by

$$\frac{dz_i}{dt} = v, \tag{1}$$

and the element remains sticking until $z_i = s_i(v)$.

Rule 2: When the element slips, the state equation is given by

$$\frac{dz_i}{dt} = \text{sgn}(v) C_i \left(1 - \frac{z_i}{s_i(v)}\right), \tag{2}$$

and the element remains slipping until the velocity passes through zero. This form of the

state equation is obtained by considering best fits, of a selected class of candidate forms, to simulation runs of the GFM.

In (2), C_i is the attraction parameter, which determines how fast z_i converges to s_i, and $s_i(v)$ is the velocity-weakening Stribeck function for i-th element. When $s_i(v)$ is replaced by the constant value W_i, corresponding to Coulomb friction, the GMS model reduces to the usual Maxwell-slip model.

The friction force of the GMS model is the sum of the outputs of the N elementary state models plus two extra terms to account for unmodeled effects, that is,

$$F_f(t) = \sum_{i=1}^{N} (k_i z_i(t) + \sigma_i \dot{z}_i(t)) + f(v).$$

The term $k_i z_i(t)$ is the elasto-sliding friction force, while $\sigma_i \dot{z}_i(t)$ represents possible viscoelastic behavior. Finally, $f(v)$ is the velocity-strengthening, that is, the viscous component, which is usually chosen to be proportional to $v(t)$.

For identification based on the GMS model, the number of unknown parameters in the model depends on the number of Maxwell elements. Each element is characterized by a stiffness k_i, a viscoelastic coefficient σ_i, an attraction parameter C_i, and a velocity-weakening function $s_i(v)$. The function $s_i(v)$ can be described by three parameters, in the form $s_i(v) = s_i(0) + (s_i(0) - s_i(\infty))(\exp(-\alpha_i v) - 1)$, where α_i is the reciprocal of the Stribeck velocity for the i-th element . In this case, we thus need to identify six parameters per element. However, we can reduce this number without sacrificing the essence of the model by assuming a common form of the velocity weakening curve for all elements, specifically, $s_i = \nu_i S$, where ν_i is a scaling parameter and $S = S(v)$ is described by three or more parameters. The same approach can be applied to the attraction parameter $C_i = \nu_i C$ in (2),

see [34], and with regard to the viscoelastic coefficient σ_i. With this latter reduction, we need to identify only two parameters per element, namely, k_i and ν_i, and five (common) parameters for the system as a whole, namely, $s(0)$, $s(\infty)$, α, C, and σ.

Finally, identification of the parameters of the GMS model can be carried out by any optimization method that is suitable for nonlinear problems, such as the downhill-simplex algorithm [35], [10]. The friction-displacement-time data used for identification must be obtained in such a way as to encompass the effects of the various friction regimes. Using a single common curve $S(v)$, it is shown in [10], [35] that as few as four Maxwell elements can provide a good fit to the data.

Properties and characteristics of the GMS friction model

The GMS model satisfies standard properties that a well-behaved friction model is expected to possess. These properties include continuity of the friction force as function of time; boundedness of the nonviscous part of the friction force by the static friction force; and dissipativity [34]. When the friction behavior predicted by the GMS model is compared with that of LuGre model, Leuven model, and the GFM, in the various regimes, namely, pre-sliding, friction lag, transition between pre-sliding and sliding, and the non-drifting property, the GMS appears to be the only model that is consistent with the GFM in regard to all properties [34]. The behavior of the GMS model shown in Figure 13. In particular, apart from the GFM, the GMS model is the only one that renders the non-drifting property consistently with experimental observation.

The GMS model can be used in motion control schemes in order to compensate for

the undesirable friction effects on the accuracy of machines. The simplest and most obvious way to do that is to include the GMS model in the feedforward part of the control loop [35], [36], [37].

COMPARISON BETWEEN MODELS AND EXPERIMENTAL OBSERVATIONS

Having presented a generic physics-based model, that is, the GFM, on the one hand and a empirically derived model, that is, the GMS model, on the other, it may be pertinent to wonder as to what extent either of these models is capable of capturing experimentally observed friction behavior. We must remark, however, that owing to the fact that both models contain a large number of unknown parameters, this comparison must be viewed as being qualitative rather than quantitative. The experimental data used in these comparisons is obtained from friction force measurements carried out on a tribometer, which is a test setup for measuring friction, as described in [3].

With the foregoing remark in mind, three representative comparisons, in addition to the one presented in Figure 5, are now discussed. Figure 14 depicts pre-sliding hysteresis behavior as measured experimentally (Figure 14(a)) and as simulated by each model (figures 14(b) and 14(c)), with ad hoc tuning of the unknown parameters. One external and two internal loops are shown to demonstrate the nonlocal-memory character of the hysteresis. If desired, the unknown parameters can be tuned to achieve better quantitative agreement with the the form of the hysteresis loop.

Figure 15 compares results of friction force versus velocity, for periodic sliding, showing the friction lag phenomenon. These results are obtained in the following way. First,

a sinusoidal velocity command signal is input to the tribometer (dashed line of Figure 15(a), left). The resulting velocity signal (solid line of Figure 15(a), left) follows the command except for two intervals, which correspond to transition from and to pre-sliding. This response means that we are not able to obtain the behavior for pure sinusoidal motion. Finally, the measured true velocity is plotted against the measured friction force (Figure 15(a), right). In order to effect a reasonable comparison with the models, the essential parts of the tribometer system (including the controller) are now simulated, in Matlab software, using each model in turn to simulate the friction contact. Again, the tuning of the model parameters is carried out in an ad hoc manner, since mainly a qualitative behavior is sought. Figures 15(b) and 15(c) show the resulting force-motion curves using the GFM and GMS models, respectively.

A final comparison is afforded by Figure 16 concerning stick-slip behavior. Again, the starting point is the experiment. The sliding mass is commanded to follow a ramp input, subject to a low-gain controller. This situation results in stick-slip motion (Figure 16(a)), which is complex in behavioral detail. In particular, the spring force, which is erroneously often used in experiments to gauge the friction force, is not equal to the total force. The qualitative and quantitative differences are due to the presence of high-frequency inertia forces of the moving mass during stick-slip vibrations. The results of simulation of the system using the GFM and the GMS model in figures 16(b) and 16(c), respectively, resemble the experimental ones. These measurements and simulations reveal the intricate details of the stick-slip phenomenon, especially the high frequency, damped vibrations superimposed on the basic motion.

A more rigorous comparison can be obtained by tuning the model parameters for a large set of experimental friction data, covering different regimes, which are obtained from the

same contact configuration. The error residues, resulting from the fitting optimization process, must then attain their minimal values for the same set of model parameters, regardless of the friction regime. This procedure is followed in [10], where a wide range of friction models, including GMS, are compared for their modeling performance.

CONCLUSIONS

This article discusses the two different approaches to modeling friction dynamics, namely, physics-motivated models and empirically motivated models, lays the link between them, and presents novel versions of each type. The physical mechanisms behind the generic friction model (GFM) are explained and the different frictional types of behavior are illustrated using the GFM. These types of behavior are the hysteretic friction force as a function of the displacement in pre-sliding regime, the velocity weakening and strengthening steady-state friction curve in gross sliding regime, the lift-up and lift-down effect, the friction lag property, the transition behavior from pre-sliding to gross sliding, and the modeling of stick-slip. This article also discusses an empirically motivated friction model, called the generalized Maxwell-slip (GMS) friction model, which is derived from the GFM. The resulting friction dynamics, simulated by both models, corresponds qualitatively well, in behavioral detail, with the experimentally observed friction behavior. Thus, we believe that the presented models provide a faithful description of friction force dynamics in its broad lines. Finally, possible refinement and extensions of the models have been outlined.

ACKNOWLEDGMENTS

This article presents research results of the K.U.Leuven's Concerted Research Action GOA/05/10. This research is also supported by the fund for Scientific Research-Flanders (F.W.O.) under Grant FWO4283. The work is also sponsored by the Belgian Network DYSCO (Dynamical Systems, Control, and Optimization). The scientific responsibility is assumed by its authors.

REFERENCES

[1] B. Persson, *Sliding Friction: Physical Principles and Applications*. Berlin and Heidelberg: Springer-Verlag, 1998.

[2] B. Armstrong-Hélouvry, *Control of Machines with friction*. Kluwer Acacemic Publishers, 1991.

[3] V. Lampaert, F. Al-Bender, and J. Swevers, "Experimental characterisation of dry friction at low velocities on a developed tribometer setup for macroscopic measurements," *Tribology Letters*, vol. 16, no. 1, pp. 95–105, 2004.

[4] T. Baumberger, "Dry friction dynamics at low velocities," in *Physics of Sliding Friction*, B. Persson and E. Tosatti, Eds. The Netherlands: Kluwer Academic Publishers, 1996, pp. 1–16.

[5] R. Hensen and R. van de Molengraft, "Friction induced hunting limit cycles: An event mapping approach," in *Proceedings of the American Control Conference*, Anchorage, AK, May 8-10, 2002, pp. 2267– 2272.

[6] R.-H. Wu and P.-C. Tung, "Studies of stick-slip friction, presliding displacement, and hunting," *Transactions of the ASME, Journal of Dynamic Systems, Measurement, and Control*, vol. 124, pp. 111–117, 2002.

[7] F. Al-Bender, V. Lampaert, and J. Swevers, "A novel generic model at asperity level for dry friction force dynamics," *Tribology Letters*, vol. 16, no. 1, pp. 81–93, 2004.

[8] B. Bhushan, *Handbook of Micro/Nano Tribology*, 2nd ed. CRC Press, Boca Raton, 1999.

[9] R. Burridge and L. Knopoff, "Model and theoretical seismicity," *Bull. Seismol. Soc. Am.*, vol. 57, no. 3, pp. 341–371, 1967.

[10] K. Worden, C. X. Wong, U. Parlitz, A. Hornstein, D. Engster, T. Tjahjowidodo, F. Al-

Bender, D. D. Rizos, and S. D. Fassois, “Identification of pre-sliding and sliding friction dynamics: Grey box and black-box models,” *Mechanical Systems and Signal Processing*, vol. 21, no. 1, pp. 514–534, 2007.

[11] N. Gitis and L. Volpe, “Nature of static friction time dependence,” *J. Phys. D*, vol. 25, no. 4, pp. 605–612, 1992.

[12] H. Czichos, *Tribology, a system approach to the science and technology of friction, lubrication and wear*, 2nd ed. Elsevier, Amsterdam, 1979.

[13] F. P. Bowden and D. Tabor, *The Friction and Lubrication of Solids, part II*. Clarendon Press, Oxford, 1964.

[14] J. Greenwood and J. Williamson, “Contact of nominally flat surfaces,” *Proc. R Soc. London, Ser. A*, vol. 295, pp. 300–319, 1966.

[15] S. Björklund, “A random model for micro-slip between nominally flat surfaces,” *Trans. ASME, J. Tribology*, vol. 119, no. 4, pp. 726–732, 1997.

[16] G. Tomlinson, “A molecular theory of friction,” *Philos. Mag. Ser.*, vol. 7, no. 7, pp. 905–939, 1929.

[17] C. Coulomb, “Theorie des machines simples, en ayant egard au frottement de leurspar-ties, et a la roideur ddews cordages,” *Memorie de Mathematique et de Physics de l’academie Royal*, pp. 161–342, 1785.

[18] D. Dowson, *History of Tribology*. Longman Ltd., London, 1979.

[19] J. Swevers, F. Al-Bender, C. Ganseman, and T. Prajogo, “An integrated friction model structure with improved presliding behaviour for accurate friction compensation,” *IEEE trans. on Automatic Control*, vol. 45, no. 4, pp. 675–686, 2000.

[20] P. Rogers and G. Boothroyd, “Damping at metallic interfaces subjected to oscillating tangential loads,” *Trans. ASME, J. Engng Ind.*, pp. 1087–1093, 1975.

[21] S. Futami, A. Furutani, and S. Yoshida, “Nanometer positioning and its micro-dynamics,” *Nanotechnology*, vol. 1, no. 1, pp. 31–37, 1990.

[22] F. Al-Bender, W. Symens, J. Swevers, and H. Van Brussel, “Theoretical analysis of the dynamic behavior of hysteresis elements in mechanical systems,” *International Journal of Non-linear Mechanics*, vol. 39, pp. 1721–1735, 2004.

[23] E. Rabinowicz, *Friction and Wear of Materials*. New York: Wiley, 1965.

[24] D. Hess and A. Soom, “Friction at a lubricated line contact operating at oscillating sliding velocities,” *Trans. ASME, J. Tribology*, vol. 112, no. 2, pp. 147–152, 1990.

[25] J. Rice and A. Ruina, “Stability of steady frictional slipping,” *Trans. ASME, J. Appl. Mech.*, vol. 50, pp. 343–349, 1983.

[26] R. Kappagantu and B. Feeny, “Proper orthogonal modes of a beam with frictional excitation,” in *Series on Stability, Vibration and Control of Systems: Series B, vol 14*, A. Guran, Ed. World Scientific, 1998, ch. Impact and friction of solids, structures and intelligent machines, pp. 167–172.

[27] W. Symens and F. Al-Bender, “Characterisation of frictional hysteresis in ball-bearing guideways,” *Wear*, vol. 258, no. 11-12, pp. 1630–1642, 2005.

[28] F. Al-Bender and W. Symens, “Dynamic characterization of hysteresis elements in mechanical systems: I. theoretical analysis,” *Chaos: An Interdisciplinary Journal of Nonlinear Science*, vol. 15, Article ID 013105, 2005.

[29] W. Symens and F. Al-Bender, “Dynamic characterization of hysteresis elements in mechanical systems: II. experimental validation,” *Chaos: An Interdisciplinary Journal of Nonlinear Science*, vol. 15, Article ID 013106, 2005.

[30] F. Al-Bender and K. De Moerlooze, “A model of the transient behavior of tractive rolling contacts,” *Advances in Tribology*, Article ID 214894, doi:10.1155/2008/214894,

2008.

[31] K. De Moerlooze and F. Al-Bender, “Experimental investigation into the tractive pre-rolling behavior of balls in v-grooved tracks,” *Advances in Tribology*, Article ID 561280, doi:10.1155/2008/561280, 2008.

[32] F. Al-Bender, V. Lampaert, and J. Swevers, “The generalized maxwell-slip model: a novel model for friction simulation and compensation,” *IEEE Transactions on Automatic Control*, vol. 15, no. 11, pp. 1883–1887, 2005.

[33] V. Lampaert, J. Swevers, and F. Al-Bender, “Modification of the Leuven integrated friction model structure,” *IEEE Trans. Automatic Control*, vol. 47, no. 4, pp. 683–687, 2002.

[34] V. Lampaert, F. Al-Bender, and J. Swevers, “A generalized maxwell-slip friction model appropriate for control purposes,” in *Proceedings of the 3rd European Control Conference*, St. Petersburg, Russia, August 2003, pp. 1170–1178.

[35] T. Tjahjowidodo, F. Al-Bender, H. Van Brussel, and W. Symens, “Friction characterization and compensation in electro-mechanical systems,” *Journal of Sound and Vibration*, vol. 308, no. 3-5, pp. 632–646, 2007.

[36] V. Lampaert, J. Swevers, and F. Al-Bender, “Comparison of model and non-model based friction compensation techniques in the neighbourhood of pre-sliding friction,” in *Proceedings of the American Control Conference*, Boston, June, 2004, pp. 1121–1126.

[37] Z. Jamaludin, H. Van Brussel, and J. Swevers, “Quadrant glitch compensation using friction model-based feedforward and an inverse-model-based disturbance observer,” in *Proceedings of the 10th Workshop on Advanced Motion Control*, Trento, Italy, March 26-28, 2008, pp. 212–217.

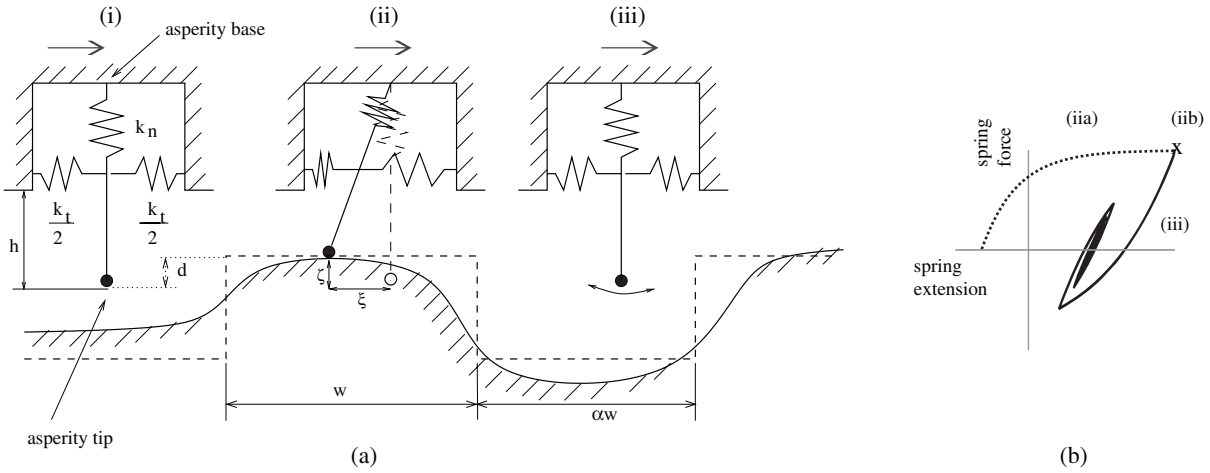

Figure 1. Asperity contact scenario. (a) Life cycle of an average asperity contact. The asperity mass is lumped into one point (●) supported by tangential and normal springs. This point is initially moving freely (i) until it touches the lower rigid surface (ii). After sticking and slipping, it breaks completely loose from the lower profile (iii). (b) depicts the force-deformation diagram during a contact cycle; where (iia) is the stick phase, (iib) is the slip phase, and (iii) is free vibration after breaking loose from the lower profile. Upon breaking loose, the asperity is assumed to dissipate all of its elastic energy through internal hysteresis losses.

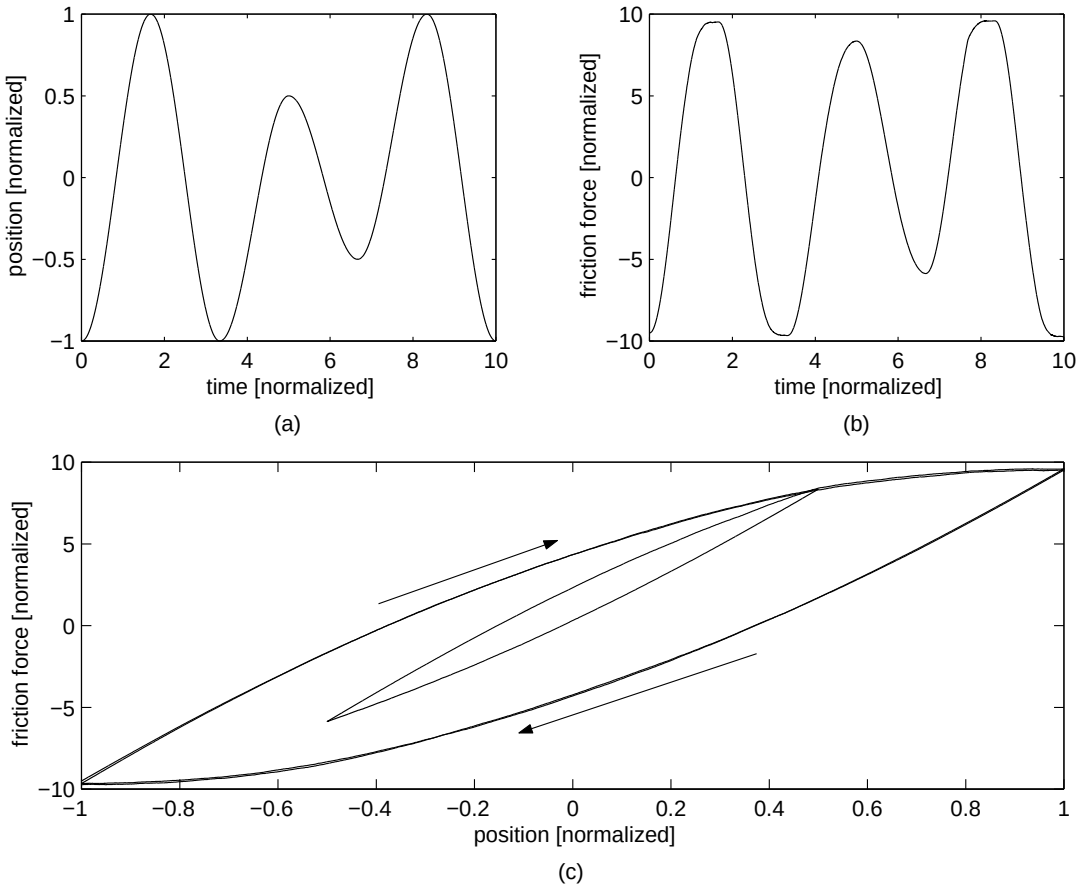

Figure 2. Simulation results of the GFM in the pre-sliding regime. (a) and (b) show the imposed displacement and the resulting force. (c) shows the corresponding rate-independent hysteresis loops with nonlocal memory obtained by plotting the force as a function of the displacement.

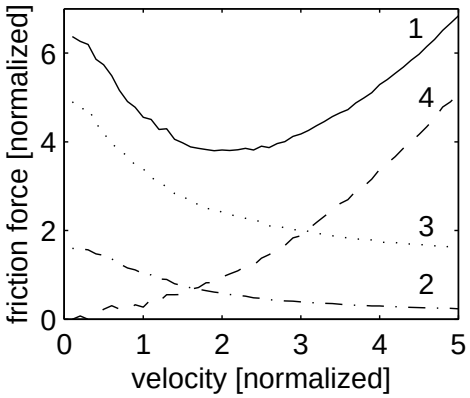

Figure 3. Friction force as function of the velocity. The steady-state friction-velocity curve, that is, the Stribeck curve (curve 1), and its various components. Curve 2 is the component due to the deformation of the asperities. Curve 3 is the component due to the adhesion forces. Curve 4 is the component due to impact of the asperity masses. Curves 2 and 3 pertain to velocity weakening, while curve 4 pertains to velocity strengthening

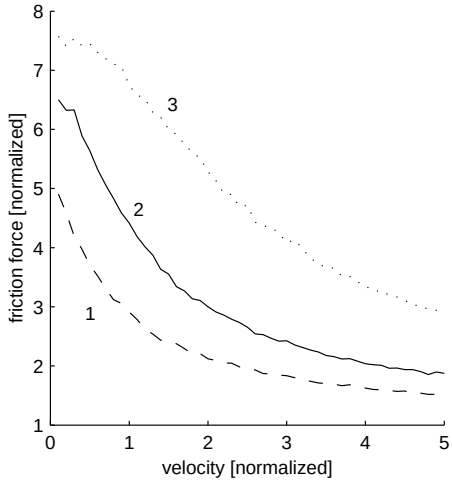

Figure 4. Velocity weakening in steady-state sliding, as simulated by the GFM. These curves illustrate the influence of the tangential stiffness of the asperities on the velocity-weakening behavior. Cases 1, 2, and 3 correspond to decreasing mean tangential stiffness. An increase in the tangential asperity stiffness results in a lower elastic energy during deformation and hence a lower friction level.

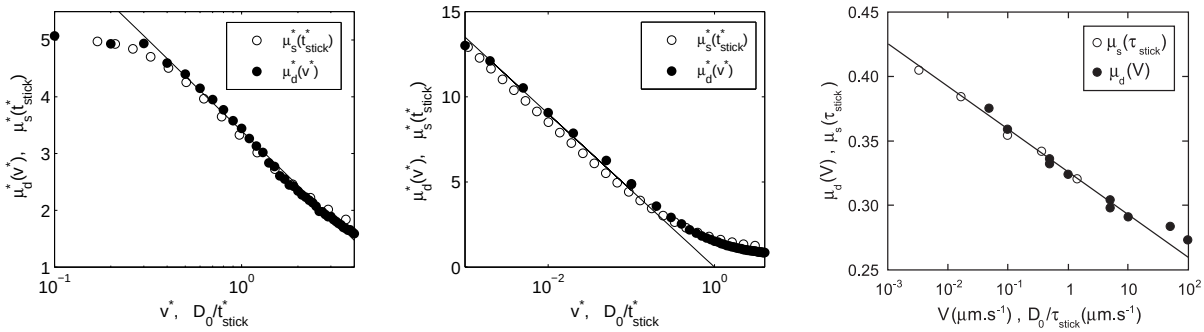

Figure 5. Correlation of the local adhesion coefficient, as a function of time, with the sliding coefficient of friction as a function of the velocity. (a) and (b) show simulation results using the GFM with an exponential and a logarithmic local adhesion coefficient curve, respectively. The dots correspond to the normalized friction force (friction coefficient) as a function of the normalized velocity, the crosses correspond to the normalized adhesion coefficient as a function of rest (dwell) time. The solid line corresponds to a fitted logarithmic law of the form $A + B\ \log(v)$. (c) shows experimental results reproduced from [4].

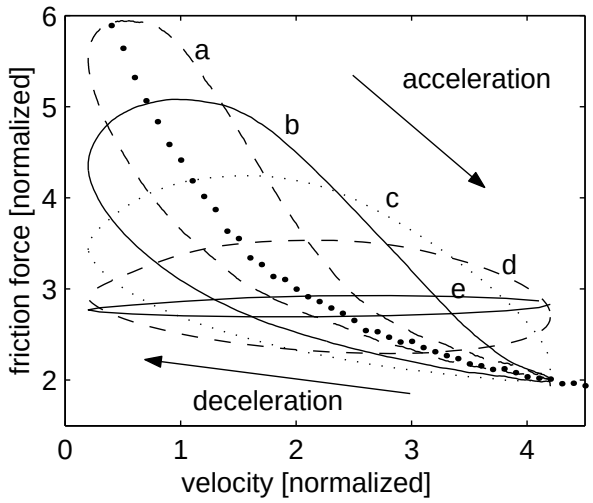

Figure 6. The friction force as a function of the velocity for non-steady-state velocities. The large dots represent the steady-state friction-velocity (weakening) curve. The friction-lag behavior is shown by the loops a, b, c, d, and e, corresponding to the dimensionless frequencies of 0.1, 0.25, 0.5, 1, and 5, respectively. For low frequencies, the loops remain close to the steady-state curve; the departure becomes more and more significant as the frequency increases.

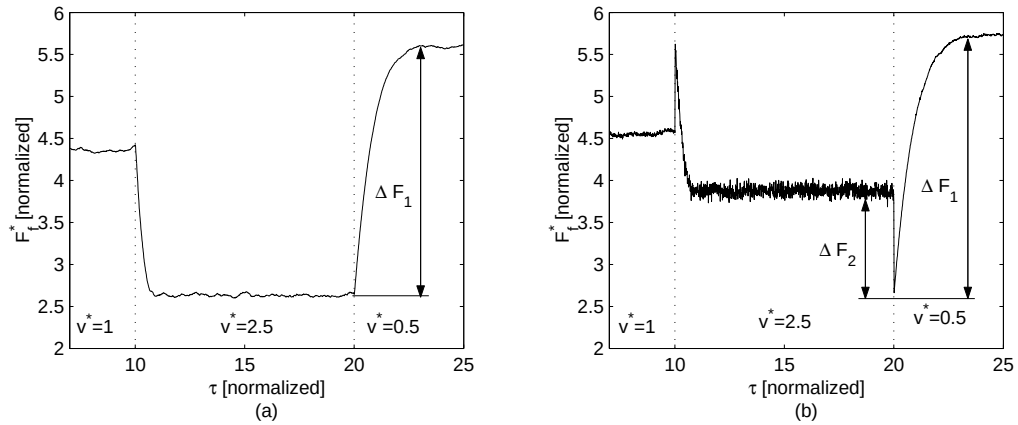

Figure 7. The normalized friction force as a function of the normalized time for two different velocity step sizes, namely, a velocity step equal to $+1.5$ and a step equal to -2. (a) shows the response without the asperity mass interaction, that is, without the viscous effect. (b) shows the response with asperity mass interaction, that is, including the viscous effect. ΔF_1 corresponds to the evolving friction change, while ΔF_2 corresponds to the instantaneous friction change for a velocity step arising from the viscous effect.

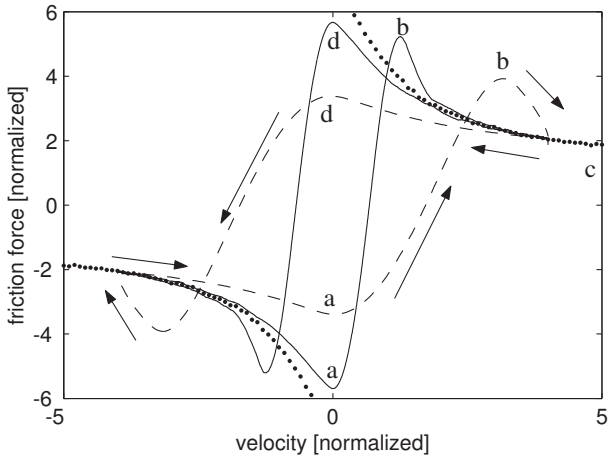

Figure 8. The friction force as a function of the relative velocity under sinusoidal excitation using a low (solid line) and a high (dashed line) frequency. The dots correspond to the velocity-weakening curve. Friction lag is observed, as well as the crossover at velocity reversals, where the motion passes through pre-sliding. When the velocity goes through zero (a), the direction of motion is reversed, and all of the active asperities are relaxed and reloaded in the new direction of displacement. The friction force increases until it reaches a maximum value (b), called the breakaway force, lying above the steady-state curve. From the moment of breakaway, the object is in gross sliding and the friction force is attracted to the steady-state curve. As in the case of friction lag, the steady-state curve lies between the curves of acceleration ($b - c$) and deceleration ($c - d$).

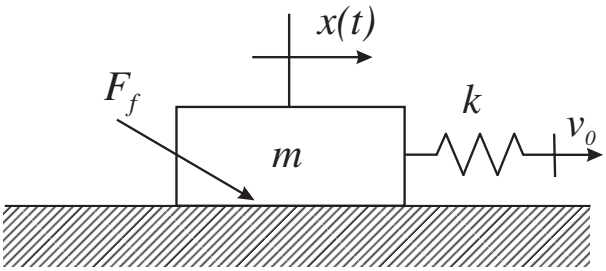

Figure 9. Schematic setup to investigate stick-slip. The block is connected to a spring whose free end is driven with a constant velocity v_0.

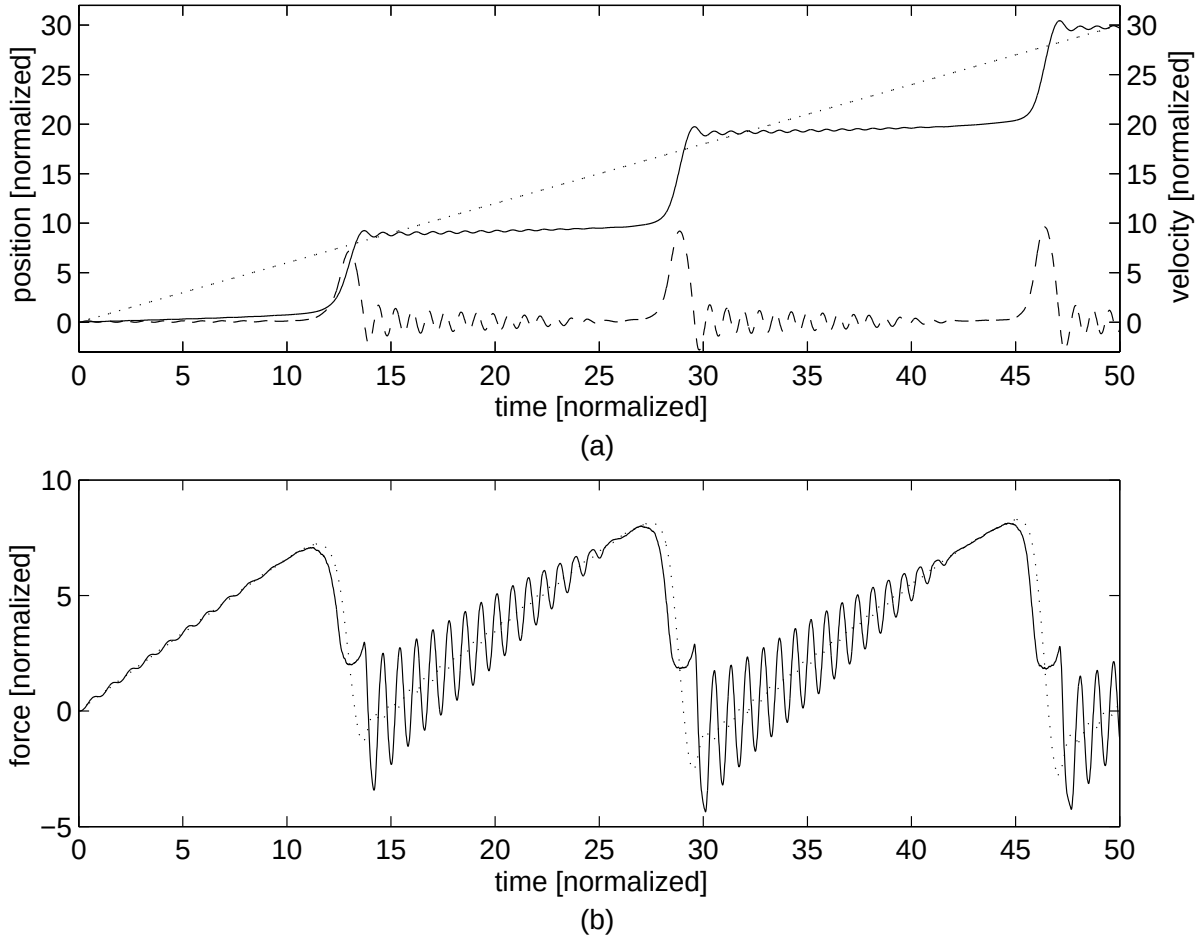

Figure 10. Stick-slip behavior. (a) shows the desired position (dotted line), the actual position (solid line), and the actual velocity (dashed line) as a function of time. (b) shows the applied force to the mass (dotted line) and the friction force (solid line) as a function of time. The object sticks until the friction force equals the breakaway force. As the block begins to slide, the increasing velocity results in a decreasing friction force. At the same time the applied (spring) force also decreases because the desired velocity is smaller than the actual velocity of the block. The block accelerates until the friction force equals the spring force. From that moment on, the block decelerates, resulting in a higher friction force, which maintains this process until the block sticks again. During the stick period a characteristic damped oscillatory behavior in the pre-sliding regime occurs. The instantaneous frequency of this oscillation is determined by the mass of the moving object, the total stiffness of the spring, and the contact stiffness in the pre-sliding regime.

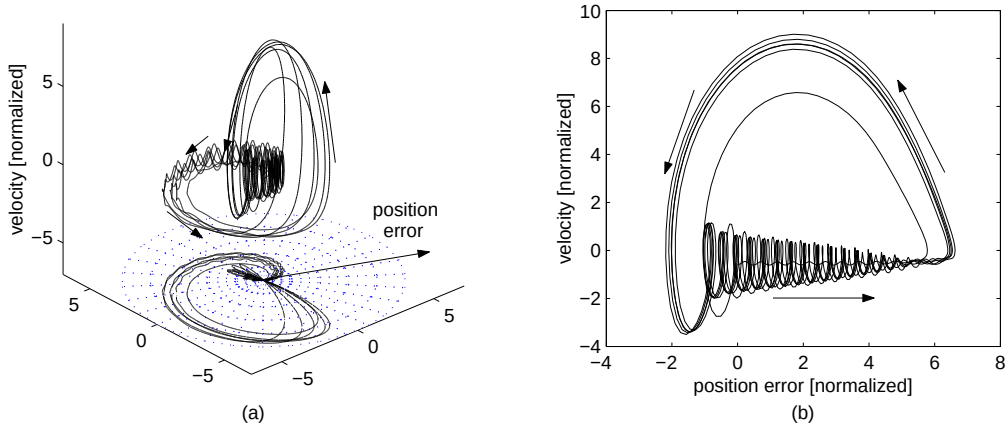

Figure 11. Phase plot representations of stick-slip motion. (a) shows the time history of the states (displacement and velocity) during stick-slip, plotted in cylindrical coordinates, with displacement as the radial axis, velocity as the longitudinal axis, and time as the circumferential coordinate. (b) The phase portrait corresponding to (a).

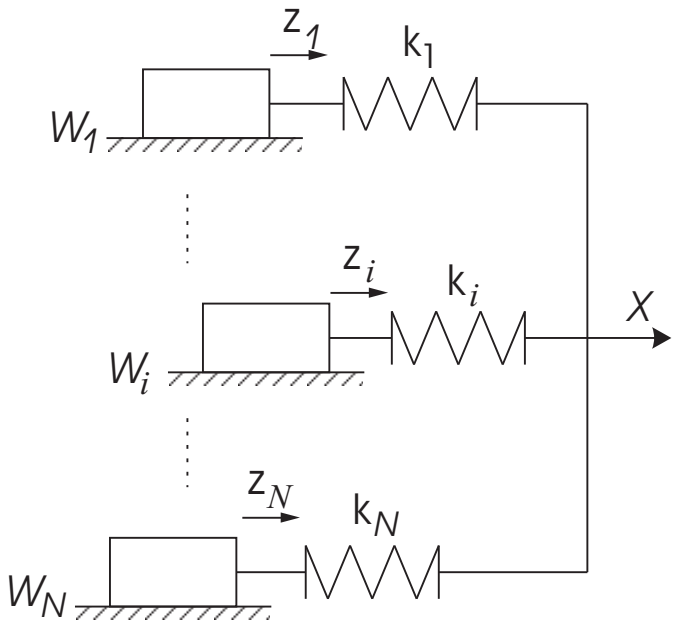

Figure 12. Representation of the Maxwell-slip friction model using N elementary models, which are friction blocks connected through linear springs. Each block is in a state of either stick or slip depending on whether the spring force, $k_i(X - z_i)$ exceeds the friction force W_i. When the motion is reversed, each block sticks immediately. When the friction law during slip is that of Coulomb, the classical Maxwell slip model is obtained. When a rate-state friction model is used, the generalized Maxwell slip (GMS) model is obtained.

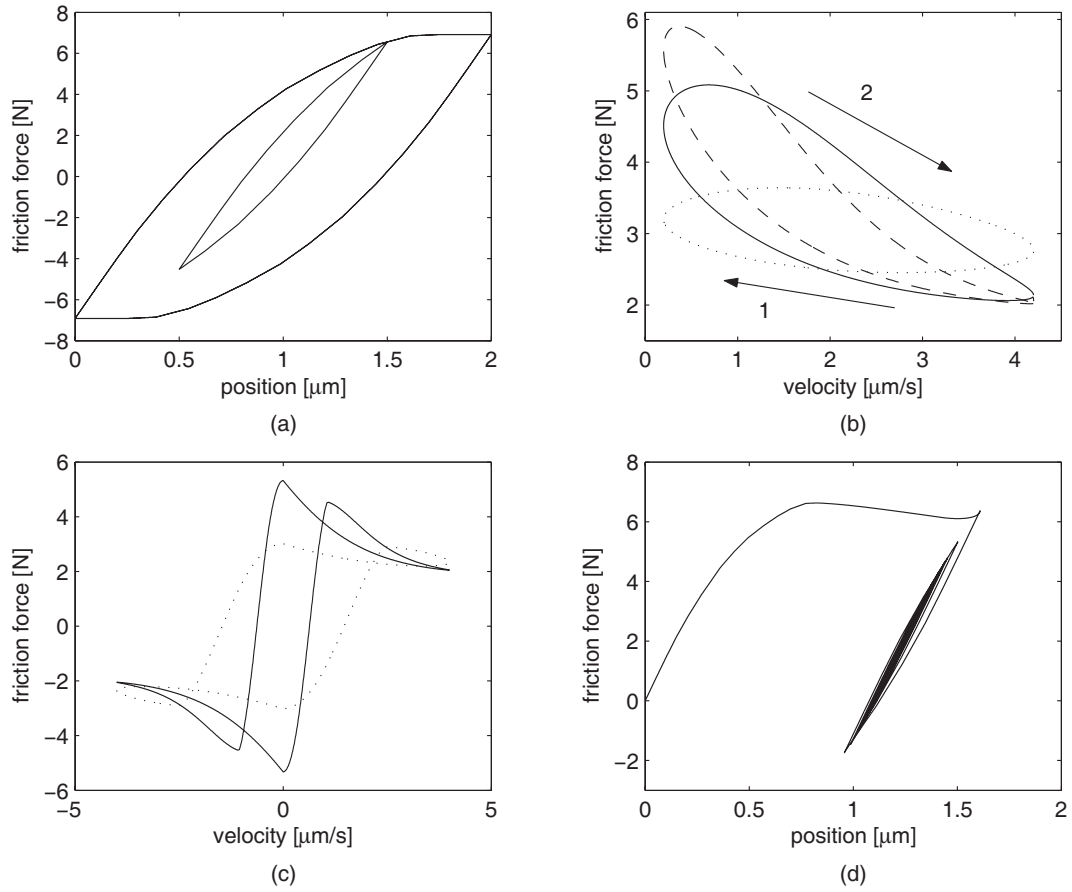

Figure 13. The friction behavior of the GMS friction model. (a) shows the (rate-independent) hysteresis with nonlocal memory in the pre-sliding. (b) shows friction lag with increasing acceleration (dashed = arbitrary datum value , solid = $\times 16$, dotted = $\times 100$). (c) shows periodic-motion friction with sliding, with the frequency changing by a factor of 10 between solid and dotted. (d) shows the non-drifting property, which is the response to an oscillatory force input, after sliding, whose amplitude remains under the breakaway limit.

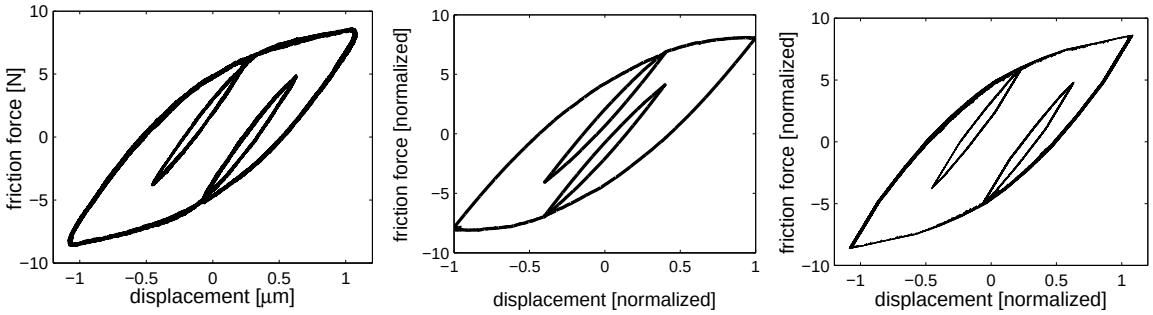

(a) (b) (c)

Figure 14. Pre-sliding hysteresis behavior given by both measurement and simulation. (a) shows pre-sliding hysteresis measured by means of a tribometer. (b) and (c) show simulated pre-sliding hysteresis using the GFM and GMS models, respectively. The measured behavior and modeled behavior, using either the micro or macro model, agree qualitatively.

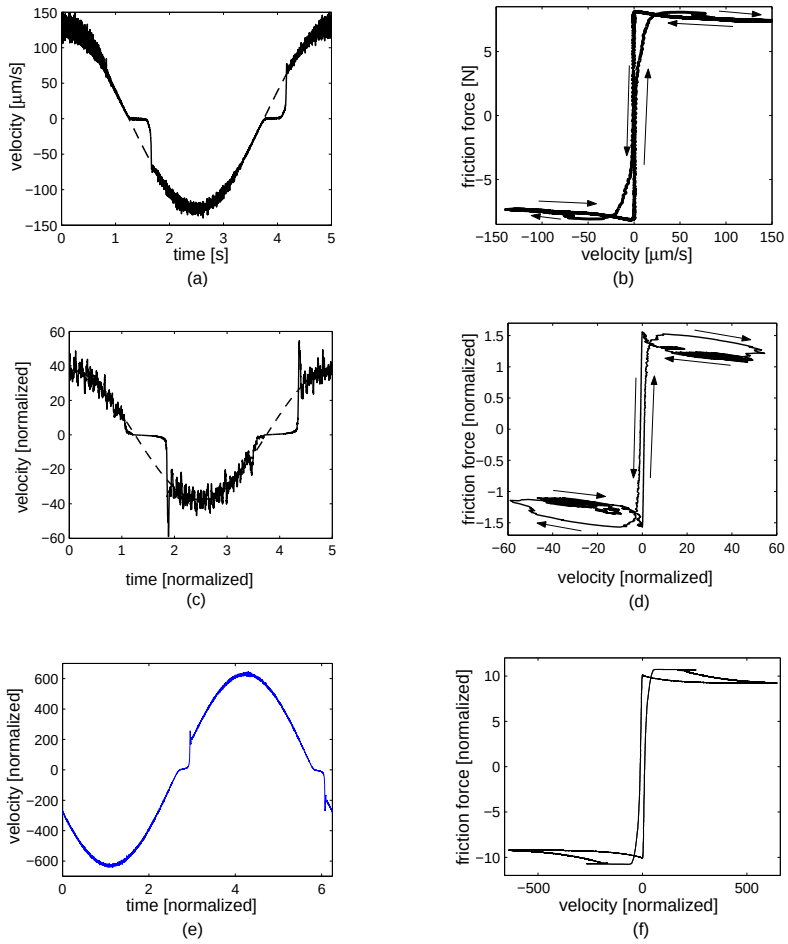

Figure 15. Periodic sliding behavior measurement and simulation. (a) and (b) show measurement from a tribometer tribometer, (a) is the measured relative velocity, while (b) is the friction force plotted as a function of the relative velocity. (c) and (d) show simulation results using the GFM, (c) is the relative velocity, while (d) is the friction force plotted as a function of the relative velocity. (e) and (f) show simulation results using the GMS model, (e) is the relative velocity, while (f) is the friction force plotted as a function of the relative velocity. The dashed curves in (a) and (c) represent the velocity command, while the solid lines are the actual velocity, which shows a departure from the command around motion reversal points owing to pre-sliding effects. The tuning of the model parameters is carried out in a trial-and-error manner.

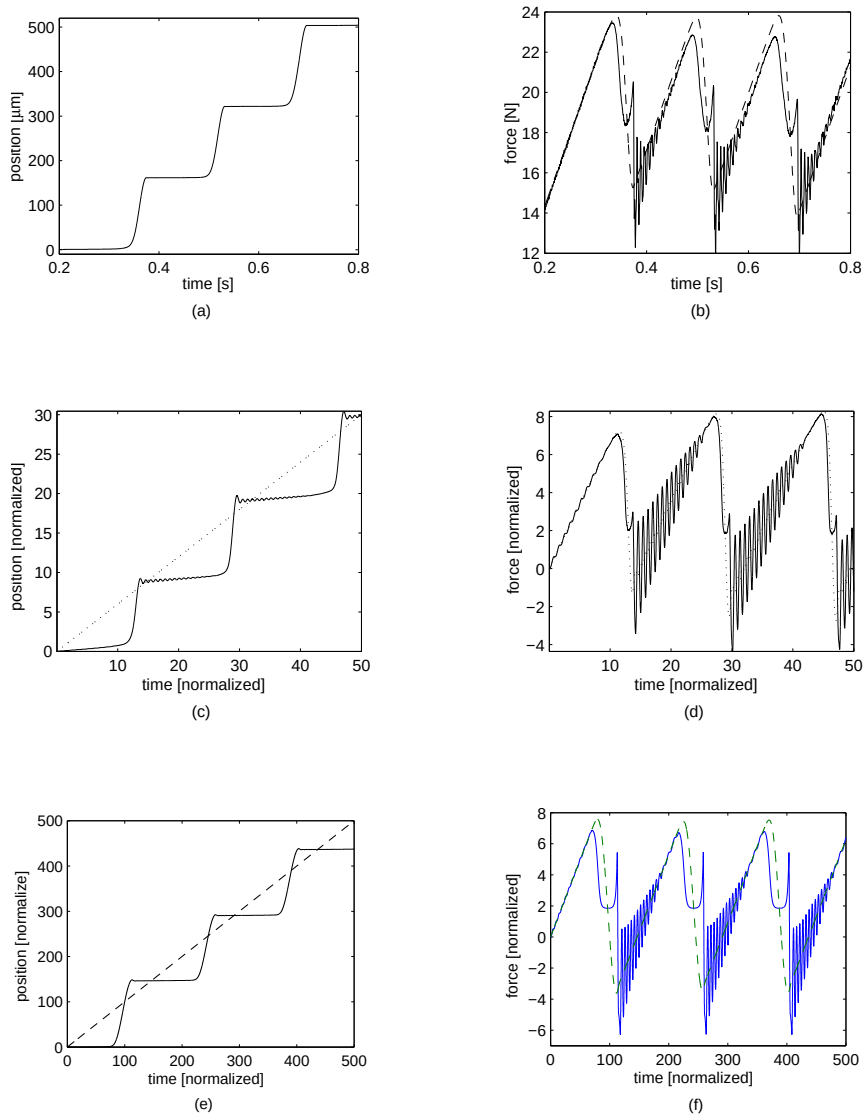

Figure 16. Stick-slip behavior measurement and simulation. The sliding mass is commanded to follow a position ramp (constant velocity) input, subject to a low-gain controller. This situation results in stick-slip motion, (a) and (b),in the experiment as well as in the simulations, where (c) and (d) show simulations using the GFM, and (e) and (f) show simulations using the GMS model. The stick-slip motion is complex in behavioral detail. In particular, the spring force, represented by the dashed lines in figures (b), (d) and (f), is not equal to the total force, plotted as solid lines on the same figures. The simulation results qualitatively resemble the experimental ones, especially the high frequency, damped vibrations superimposed on the spring force curves in figures (b), (d), and (f).

SIDEBAR S1: PHYSICS-MOTIVATED FRICTION MODELS

The various physics-motivated friction models analyzed in the literature can be divided into three classes according to the scale of approach. *Asperity-scale* models are common in the control domain, while *tectonic-plate-scale* and *atomic-molecular-scale* models belong to the geophysics and nanotechnology communities, respectively. However, despite the wide range of scales of approach, a similarity underlies all three classes.

According to [18], Coulomb is perhaps the first researcher to offer an explanation for the difference between static and kinetic friction by considering asperity interaction. Realizing that surfaces are not ideally flat and are formed by asperities, he reasons that the interlocking of asperities can be a source of friction force as well as the disparity between static and kinetic friction forces. Recognizing the presence of asperities and the existence of interfacial forces, it is argued that adhesion occurs at asperity surfaces and that shearing occurs upon translational motion [13]. This model explains the disparity between true area of contact and apparent area of contact as well as the relation between the friction force and load, since the asperities and thus the true area of contact change with load.

The dynamics of asperity interaction can also be considered. Surface asperities can, in principle, be likened to the bristles of a brush. When the bristles are endowed with physical properties, dynamical friction models can be derived [S1], [S2],[33]. Based on this idea, [S1] develops a bristle model that tries to simulate friction in the pre-sliding as well as in the sliding regime. The physical paradigm underlying the bristle model is a pair of facing surfaces with deformable bristles extending from each surface, where the friction interaction occurs at the bristle tips.

In the geophysics community, at tectonic scale, it has been suggested that earthquakes might be caused by stick-slip instabilities in the relative sliding of tectonic plates [S3]. The use of computational simulation of earthquake activity as a strategy for understanding seismicity began in 1967 [9], where a vertical strike-slip fault in the Earth's crust is modeled as a one-dimensional string of sliding blocks with masses m connected to one another by springs with stiffness k_c (see Figure S1). In this model, the buildup of tectonic forces is represented by the externally driven motion of a loader plate, which is connected to the blocks through springs k_t. The main feature of the local friction function F_f is a sudden decrease as the velocity deviates from zero such that the system is in a condition of dynamic instability during the shock.

Since the invention of the atomic force microscope, research on the physics behind friction force at the atomic scale has intensified. The classical molecular and atomic models are described in [S4], [S5]. The basic outline of the various models and methods is straightforward. First, an interaction periodic potential V_E, such as the Lennard-Jones potential, sine-wave potentials, or simple ideal springs, is defined. This potential produces forces on the individual particles, typically atoms or molecules, whose dynamics are followed. Next, the geometry and boundary conditions are specified, and initial coordinates and velocities are given to each particle. The equations of motion for the particles are then integrated numerically, stepping forward by discrete steps [S4].

Models that simulate wearless friction in low-dimensional systems include the Tomlinson model [16], the Frenkel-Kontorova model [S6], [S7], [S8], [S9], [S10], [S11], and a combination of the models, known as the Frenkel-Kontorova-Tomlinson model [S12]. These models are similar to the Knopoff-Burridge model, where the masses correspond with

atoms or molecules. The main difference is that the phenomenological friction law for F_f is replaced by an atomic realization [S13]. The original models are special cases of this model. For example, Tomlinson's atomic model [16] has no springs that interconnect the atoms ($k_c = 0$), while the Frenkel-Kontorova model has no springs connected to the upper surface ($k_t = 0$) except the first spring. In [16] a dissipation mechanism of wearless sliding friction is advanced, based on one surface plucking the atoms of the other surface, thus causing them to vibrate and dissipate energy through the bulk material. The underlying idea is in fact also applicable to asperity interaction during sliding, in other words, on a scale that is larger than the atomic. Two additional aspects must be included in this case, namely, adhesion and creep.

REFERENCES SIDEBAR 1

[S1] D. A. J. Haessig and B. Friedland, "On the modeling and simulation of friction," *Trans. ASME, J. of Dynamic Systems, Measurements and Control*, vol. 113, no. 3, pp. 354–362, 1991.

[S2] C. Canudas de Wit, H. Olsson, K. Aström, and P. Lischinsky, "A new model for control of systems with friction," *IEEE Trans. Automatic Control*, vol. 40, no. 5, pp. 419–425, 1995.

[S3] B. Feeny, A. Guran, N. Hinrichs, and K. Popp, "A historical review on dry friction and stick-slip phenomena," *ASME Appl. Mech. Rev.*, vol. 51, no. 5, pp. 321–341, 1998.

[S4] B. Bhushan, *Modern Tribology Handbook*. CRC Press LLC, 2001.

[S5] D. Frenkel and B. Smit, *Understanding Molecular Simulation: From Algorithms to Applications*. Academic Press, San Diego, 1996.

[S6] Y. I. Frenkel and T. Kontorova, "On the theory of plastic deformation and twinning," *Zh. Eksp. Theor. Fiz. (USSR)[Sov. Phys. JETP 13,1(1938)]*, vol. 8, no. 1, pp. 1340–1349, 1938.

[S7] Y. Braiman, H. G. E. Hentschel, F. Family, C. Mak, and J. Krim, "Tuning friction with noise and disorder," *Phys. Rev. E*, vol. 59, no. 5, pp. R4737–R4740, 1999.

[S8] M. Paliy, O. Braun, T. Dauxois, and B. Hu, "Dynamical phase diagram of the dc-driven underdamped Frenkel-Kontorova chain," *Phys. Rev. E*, vol. 56, no. 4, pp. 4025–4030, 1997.

[S9] H. Matsukawa and H. Fukuyama, "Theoretical study of friction: One dimensional clean surfaces," *Phys. Rev. B*, vol. 49, pp. 17 286–17 292, 1994.

[S10] T. Strunz and F.-J. Elemer, "Driven Frenkel-Kontorova model: I. uniform sliding states and dynamical domains of different particle densities," *Phys. Rev. E*, no. 58, pp. 1601–

1601, 1998.

[S11] ——, “Driven Frenkel-Kontorova model: II. chaotic sliding and nonequilibrium melting and freezing,” *Phys. Rev. E*, no. 58, pp. 1612–1622, 1998.

[S12] M. Weiss and F. J. Elmer, “Dry friction in the Frenkel-Kontorova-Tomlinson model: Static properties,” *Phys. Rev. B*, vol. 53, pp. 7539–7549, 1996.

[S13] F.-J. Elmer, “Is self-organized criticality possible in dry friction?” in *Physics of Sliding Friction*, B. Persson and E. Tosatti, Eds. Dordrecht: Kluwer Academic Publishers, 1996, pp. 433–447.

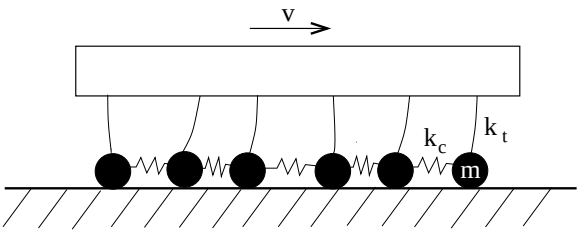

Figure S1. Schematic of the Burridge-Knopoff model. A vertical strike-slip fault in the Earth's crust is modeled as a one-dimensional string of sliding blocks with masses m connected to one another by springs with stiffness k_c and to the loader plate through springs with stiffness k_t.

SIDEBAR S2: GENERALIZED EMPIRICAL FRICTION MODEL STRUCTURE

In the class of generalized empirical friction models, the friction force F_f is a generalized function of an internal state vector $\mathbf{z}$, the relative-sliding velocity v, and the position x of the moving object, that is,

$$F_f = \mathcal{F}(\mathbf{z}, v, x). \tag{S1}$$

The state equation that describes the dynamics of the internal state vector $\mathbf{z}$ is a first-order differential equation of the form

$$\frac{d\mathbf{z}}{dt} = \mathcal{G}(\mathbf{z}, v, x). \tag{S2}$$

In (S1) and (S2), $\mathcal{F}(\cdot)$ and $\mathcal{G}(\cdot)$ are general nonlinear functions. In particular, $\mathcal{G}(\cdot)$ may be discontinuous so that both pre-sliding and gross sliding can be represented.

Reference [25] shows, in particular, that $\mathcal{F}(\mathbf{z}, v, x) = F_1(\mathbf{z}, v, x) + F_2(v)$, where F_1 is responsible for the transient velocity response, accounting for the Stribeck effect and friction lag, while F_2 represents the instantaneous response to velocity changes, that is, the viscous effect. However, this formulation corresponds to sliding, and thus does not allow for pre-sliding or for passing through zero velocity.

The objective of empirical friction modeling is to find suitable expressions for the generalized functions $\mathcal{F}(\cdot)$ and $\mathcal{G}(\cdot)$, such that the resulting model faithfully simulates all observed types of friction behavior.

Two generic considerations provide limiting conditions on the functions $\mathcal{F}(\cdot)$ and $\mathcal{G}(\cdot)$. First, for constant velocities, the steady-state ($d\mathbf{z}/dt = 0$) friction force is a function of

only the velocity v. Thus, if v is constant, then

$$\mathcal{G}(\mathbf{z}, v, x) = 0 \tag{S3}$$

and

$$\mathcal{F}(\mathbf{z}, v, x) = F(v) = s(v) + F_2(v), \tag{S4}$$

where $s(v)$ is the velocity-weakening curve, while $F_2(v)$ is the viscous, that is, velocity-strengthening curve.

The second condition on the general functions is determined by the frictional behavior in the pre-sliding regime at small displacements. The friction force is then a hysteresis function of the position, with nonlocal memory characteristics [19] given by

$$F_f = \mathcal{F}(\mathbf{z}, v, x) = F_h(x). \tag{S5}$$

SIDEBAR S3: EMPIRICALLY MOTIVATED FRICTION MODELS

Empirically motivated models are especially useful in the control domain. The requirements for such models are threefold, namely, the model must be as simple as possible to facilitate online use; it must be complex enough to describe all frictional properties that are relevant for control; and the number of parameters must be as small as possible and easy to identify.

Numerous friction models have been developed for control, varying from simple static models to complex dynamic ones. The most elementary models are the classical friction models that describe the friction force as a function of the velocity only. An early attempt to model the dynamic aspects of friction behavior by introducing a time lag and an extra equation in the case of pre-sliding displacement is made by [S14]. However, the transition from one equation describing the sliding regime behavior to another describing the pre-sliding regime behavior is not obvious and is not incorporated into the model of [S14].

In the late 1960s, the Dahl model [S15] introduced the development of dynamic friction models based on internal states. This model captures only an approximation of the pre-sliding behavior, but it is the basis for more elaborate models, such as the Bliman-Sorine model [S16] and the LuGre model [S2]. These integrated friction models incorporate a variety of phenomena into one formulation. The LuGre model is popular since it is well suited for use in theoretical calculations and it is easy to implement. More elaborate models are the elasto-plastic model [S17], the Leuven model [19], [33], and the generalized Maxwell-slip friction model [32]. This last model is discussed in more detail in a separate section of this article.

In the geomechanics community, a general empirical *rate-state* friction-dynamics law is developed, based on experiments involving a suddenly imposed step change in the velocity [25]. Such experiments suggest that the friction force response to this velocity step is a combination of an instantaneous increase with the velocity coupled with a first-order-like decay with the evolving state.

Analysis of this class reveals that most of the available empirical friction models that are used for identification and control correspond to a generalized friction model structure, see “Generalized Empirical Friction Model Structure”. In the following, we show how these empirical friction models relate to the generalized friction model.

Static friction models include the classical models of friction, such as the Coulomb model. Those models describe a static relationship between the friction force and the velocity, corresponding to (S1) and (S3), in other words, without a state equation or pre-sliding behavior. Although such models suffice for some purposes, highly accurate positioning, for example, within the micrometer range in machine-tool applications, requires more advanced modeling.

The Dahl model [S18] provides an answer to the pre-sliding problem, which appears only as a jump discontinuity in the Coulomb model. The Dahl model approximates the pre-sliding friction force by steady-state hysteresis loops, corresponding to (S5). This relationship is often formulated in differential form, as a first-order differential equation in the force and displacement, for the purpose of including additional dynamics. The Dahl model does not, however, incorporate nonlocal memory behavior, and thus is suitable only for the analysis of steady-state periodic motion with only two motion reversals per cycle.

The LuGre model [S2] develops the Dahl equation into a dynamic state equation (S2), where the state corresponds to the average deformation of the surface asperities or bristles, and supplements it with the friction force equation (S1) in a way that satisfies condition (S3) but not condition (S5). Thus, when the Stribeck curve is flat, the dynamic state equation reduces to the quasi-static Dahl equation, which has no provision for nonlocal memory effects, as mentioned above. This shortcoming leads to the phenomenon of spurious drift when an oscillatory force, smaller than the breakaway threshold, is applied to a friction block.

Since neither the Dahl model nor the LuGre model can realize the nondrifting property in pre-sliding, an extension of the LuGre model that captures that property is formulated in [S17]. This elasto-plastic friction model introduces a modification to the state equation of the LuGre model, such that an amplitude- and rate-dependent transition is effected, from pure elastic bristle deformation to the plastic deformation state corresponding to the LuGre model. Although this model ensures the elimination of spurious drift below a pre-sliding displacement limit, it does not remedy the lack of nonlocal memory.

The integrated friction model described in [19], called the Leuven model, elaborates the LuGre model further by including pre-sliding hysteresis with nonlocal memory explicitly in the formulation. This type of hysteresis, which proves to be an essential behavioral characteristic of friction, determines the model's performance in nonperiodic pre-sliding. However, incorporating the (analytic) hysteresis function F_h while maintaining the LuGre formulation is not without implementation difficulties, which makes the model less attractive. To overcome those problems, the hysteresis function F_h is replaced by a Maxwell-slip model representation in [33].

Finally, the GFM model also shows that a systematic variation in the normal force occurs with changing tangential relative motion. This *lift-up* effect entails at least one extra state equation for the normal force, which is coupled to (S1) and (S2). Such a refinement of the model structure can lead to complex dynamics, partly through the addition of an extra degree of freedom.

REFERENCES SIDEBAR 3

[S14] B. Armstrong-Hélouvry, P. Dupont, and C. Canudas De Wit, "A survey of models, analysis tools and compensation methods for the control of machines with friction." *Automatica*, vol. 30, no. 7, pp. 1083–1138, 1994.

[S15] P. Dahl, "A solid friction model," *The Aerospace Corporation, El Segundo, CA, TOR-158(3107-18)*, 1968.

[S16] P.-A. Bliman and M. Sorine, "Easy-to-use realistic dry friction models for automatic control," in *Proceedings of the 3rd European Control Conference*, Rome, Italy, 1995, pp. 3788–3794.

[S17] P. Dupont, V. Hayward, B. Armstrong, and F. Altpeter, "Single state elasto-plastic friction models," *IEEE Trans. on Automatic Control*, vol. 47, no. 5, pp. 787–792, 2002.

[S18] P. Dahl, "Measurement of solid friction parameters of ball bearings," in *Proceedings of 6th Annual Symp. on Incremental Motion, Control Systems and Devices*, Illinois, 1977, pp. 49–60.

AUTHOR INFORMATION

Farid Al-Bender (Farid.Al-Bender@mech.kuleuven.be) holds a B.Eng. degree from the University of Sheffield (UK, 1975) and an M.Sc. degree in Tribology from the University of Leeds (UK, 1976). He received the Ph.D. degree from the Katholieke Universiteit Leuven (Belgium, 1992), where he is a professor in the Department of Mechanical Engineering. He is also managing director of the company Leuven Air Bearings. His research interests include air and fluid bearings, friction and hysteresis measurement, modeling and identification, precision and active mechatronics systems, and nonlinear systems. He can be contacted at Department of Mechanical Engineering, Division PMA, Katholieke Universiteit Leuven, Celestijnenlaan 300 B, B-3001 Heverlee, Belgium.

Jan Swevers received the M.Sc. degree in electrical engineering and the Ph.D. degree in mechanical engineering from the Katholieke Universiteit Leuven (KULeuven), Belgium, in 1986 and 1992, respectively. He is a professor in the Department of Mechanical Engineering, Division Production Engineering, Machine Design and Automation (PMA), of KULeuven. His research interests include modeling, identification, and control of mechatronics systems.